Ionization distances of multiply charged Rydberg ions approaching solid surfaces

Lj. D. Nedeljković and N. N. Nedeljković*
Faculty of Physics, University of Belgrade, P.O. Box 368, Belgrade, Serbia

D. K. Božanić
Vinča Institute of Nuclear Sciences, P.O. Box 522, Belgrade, Serbia
(Received 12 May 2006; published 27 September 2006)

The ionization distances R_c^I as well as the ionization rates and eigenenergies of one-electron multiply charged Rydberg ions (core charge $Z \gg 1$, principal quantum number $n \gg 1$) approaching solid surfaces are calculated. Within the framework of a nonperturbative étalon equation method (EEM), these quantities are obtained simultaneously. The complex energy eigenvalue problem for the decaying eigenstates is solved within the critical region $R \approx R_c \approx R_c^I$ of the ion-surface distances R. This region is characterized by the energy terms localized in the vicinity of the top of an effective potential barrier, created between the ion and polarized solid. We take into account that the parabolic symmetry is preserved for $R \approx R_c$ and that the parabolic quantum numbers can be taken as approximate but sufficiently good quantum numbers. The parabolic rates, energies, and corresponding ionization distances are presented in relatively simple analytical forms. The ionization distances are compared with the results of a classical overbarrier model. Comparison of the obtained energies and rates with the available theoretical predictions of the coupled angular mode method shows good agreement. The use of the EEM for an estimation of the upper limit of the first neutralization distance in the subsequent neutralization cascade is briefly discussed.

DOI: 10.1103/PhysRevA.74.032901 PACS number(s): 34.50.Dy, 34.50.Fa, 79.20.Rf

I. INTRODUCTION

Thus far, a number of papers studying the interaction of multiply charged ions with solid surfaces were focused on experimental and theoretical studies of the neutralization dynamics of ions slowly approaching the surfaces; for a review see Ref. [1]. A series of results concerning the formation of "hollow atoms," followed by Auger electron emission and radiative deexcitation, has been obtained. Within the framework of multielectron exchange models, scenarios for stepwise neutralization of empty electronic states of the projectiles have been proposed in order to encompass the experimental findings on the detected spectra of emitted electrons and x radiation.

Physically important conclusions are possible, however, when multiply charged ions (core charge $Z \gg 1$), with one active electron occupying a certain Rydberg state (principal quantum number $n \gg 1$), approach the conducting solid surface. The filled electronic states are subjected to an intense distortion caused by the image force response of the conducting target. Even at very large ion-surface distances R, their destruction is possible through a resonant ionization mechanism. The problem of ionization of these multiply charged Rydberg ions can be treated independently of the neutralization problem; namely, for any given $Z \gg 1$, there are such Rydberg states, with sufficiently high n values, where the resonant ionization ends before the neutralization cascade has begun. In this sense the study of such a decaying system also serves for estimating the first neutralization distance for the considered ions.

In the last two decades several theoretical methods were developed, which can be principally used for an investigation of the ionization of one-electron multiply charged Rydberg ions. The proposed methods are very heterogeneous in nature; here we mention the classical overbarrier (COB) method [1,2] and its extended dynamic version [3,4], the perturbation method [5], the coupled angular mode (CAM) method [6,7], the complex scaling method (CSM) [8–11], the stabilization method [12,13], the time-dependent close-coupling technique [14,15], and the two-state vector model [16,17] in combination with the étalon equation method (EEM) [18–20].

Despite the variety of these theoretical methods, the problem of estimating the ionization distances R_c^I of multiply charged Rydberg ions still remains open. Most frequently, two physically very different definitions of R_c^I are used. According to the classical overbarrier model [1,2] the ionization distance is considered as a critical distance R_c^{class} at which the energy term "touches" the saddle point of the ion-surface potential barrier. On the other hand, in quantum models [11,16–20], particular Rydberg states ionize over a relatively narrow range of ion-surface distances R around R_c^I, where R_c^I is the position of the total ionization rate maximum.

In line with the correspondence principle, it is reasonable to expect that R_c^I is comparable to R_c^{class}. Moreover, a quantum definition of the critical distances R_c, instead of R_c^{class}, would be worthwhile. Among other things, the R_c distances are introduced to separate the classically allowed overbarrier from purely subbarrier (tunneling) transitions of an active electron in the ion-surface system. The critical region ($R \approx R_c \approx R_c^I$) of the ion-surface distance R yields the basic information about the ionization mechanism. In this sense, a quantum model must be focused on that region from the very beginning.

In practice, determining R_c^I is closely related to a search for "sufficiently good" quantum numbers in the critical re-

*Electronic address: hekata@ff.bg.ac.yu

gion $R \approx R_c \approx R_c^I$. The lack of spherical symmetry in the ion-surface system means that the spherical quantum numbers (n,l,m) cannot be used, and that the spherical functions are not the appropriate wave functions. Instead, one can use an approach which applies the superposition of these functions, characteristic of the CAM method and CSM. Actually, a classification of the states by a set of parabolic quantum numbers $\mu=(n_1,n_2,m)$ serves very well, at least formally, for some ion-surface distances. That is, for $R \approx R_c \approx R_c^I$ the parabolic symmetry is preserved and the parabolic quantum numbers can be taken as approximate but sufficiently good quantum numbers.

In the present paper, we shall apply the above cited étalon equation method, which offers the possibility of linking the R_c^I problem and the problem of sufficiently good quantum numbers. This method represents a nonperturbative asymptotic method [21,22] for solving the one-dimensional effective eigenvalue problems (with large parameters), resulting after separation of variables at sufficiently large ion-surface distances $R \approx R_c$. The corresponding original differential equations are associated with appropriate "étalon equations" whose solutions are well known and which have the same configuration of transition points (poles and turning points) as the original ones. In particular, the EEM [23] enables us to consider the ionization as a resonant electron tunneling or as an overbarrier transition in the very vicinity of the effective potential barrier top ($R \approx R_c$). The complex energy eigenvalue problem of the Hamiltonian $\hat{H}(R)$ of an active electron can be solved by imposing the outgoing wave condition inside the solid and by using scaled parabolic coordinates. The parabolic ionization rates $\Gamma_\mu(R)$ and the corresponding energy terms $\mathrm{Re}\, E_\mu(R)$ are obtained by means of complex eigenenergies. The critical distances R_c are obtained simultaneously. Two different adaptations of the EEM [18,20] have previously been used for the analysis of the ionization problem in the vicinity of the effective potential barrier top; here we shall present an extension of the EEM from the $Z=1$ case of Ref. [20] to multiply charged Rydberg ions.

The total ionization probability $P_\mu(R)$ satisfies an appropriate system of semiclassical rate equations, at least for lower ionic perpendicular velocities $v_\perp$ [24]. For sufficiently large R, Z, and n, the ionization channel can be considered as a dominant one, i.e., we obtain a simple rate equation for $P_\mu(R)$ with the rate $\Gamma_\mu(R)$. Besides, according to a simple estimation [1], for not extremely small velocities, we can retain the classical law $v_\perp = v_\perp(R)$ of the ionic motion (with the initial condition $v_\perp = v_{\perp 0}$), which includes the image acceleration of the multiply charged projectile. Under these conditions, the nonlinear screening effects of the multiply charged ion do not affect the ionic motion significantly, and the linear response of the polarized solid is reduced to the classical image forces. Using the v-dependent total ionization probability $P_\mu(R)$ we define the ionization distance R_c^I as a v-dependent quantity, $R_c^I = R_c^I(v_{\perp 0})$, in contrast to the velocity-independent critical distances R_c.

The proposed EEM enables us to obtain the values of R_c and R_c^I, as well as the parabolic rates $\Gamma_\mu(R)$ and energies $\mathrm{Re}\, E_\mu(R)$, in sufficiently accurate analytic forms. In the present paper we restrict ourselves to the high-eccentricity Rydberg states of one-electron ions. More precisely, our analysis will be focused on those electronic states characterized by lower values of the parabolic quantum number n_1 and $m=0$. Within the EEM, it is possible to establish a critical quantum number n_c, such that the condition $n \geqslant n_c$ practically ensures the one-channel character of the ionization of multiply charged Rydberg ions. The case $n < n_c$, relevant for the study of neutralization dynamics, represents a complement of the case $n \geqslant n_c$.

This paper is organized as follows. In Sec. II we shall present the theoretical basis of the ionization of multiply charged ionic projectiles in the Rydberg states, slowly approaching conducting solid surfaces. In Sec. III we shall expose explicit results of the proposed decay model of ionization; the results will be compared with the available predictions for energy and rates of the CAM method [7], as well as with the R_c^{class} of the COB model [1,2]. Also, we shall briefly observe the results obtained within our previous EEM, Ref. [18], concerning the reionization of the outgoing ionic projectile in the beam-foil geometry, by extrapolating the present model to the limiting case of intermediate velocities ($v_{\perp 0} \approx 1$ a.u.). Some concluding remarks are given in Sec. IV.

Atomic units ($e^2=\hbar=m_e=1$) will be used throughout the paper unless indicated otherwise.

II. FORMULATION OF THE PROBLEM

A. Ionization in the decay model

We consider a multiply charged Rydberg ion (pointlike core charge Z, mass M) with one active electron, approaching a solid surface with perpendicular velocity $v_\perp = v_\perp(R)$. We restrict ourselves to the critical region $R \approx R_c \gg 1$ a.u. of ion-surface distances R. The geometry of the ion-surface system is explicated in Ref. [20]. Also, the choice of potentials relevant to the EEM are extensively discussed in Sec. II A of Ref. [20].

The one-electron Hamiltonian is given by

$$\hat{H}(R) = -\frac{1}{2}\nabla^2 + U_A + U_M + U_{AM}. \tag{2.1}$$

In the moving coordinate system, located at the ionic core, with the z_A axis oriented from the surface toward the vacuum, the Coulomb potential of the ionic core is given by $U_A = -Z/r_A$. The term $U_M + U_{AM}$ in Eq. (2.1) is the surface potential of the polarized solid. For the active electron outside the solid and the ionic projectile at distance $R \approx R_c$, using the parabolic coordinates $\xi = r_A + z_A$, $\eta = r_A - z_A$, $\varphi = \arctan(y/x)$, we have [20]

$$U_M + U_{AM} = \left(-\frac{1}{4(R-\eta/2)} + \frac{Z}{2R-\eta/2} \right) \left[1 + O\left(\frac{\xi}{R}\right) \right]. \tag{2.2}$$

In the quasistationary (adiabatic) approximation the electron wave function can be considered as an eigenfunction Ψ_μ of the Hamiltonian $\hat{H}(R)$,

$$\hat{H}(R)\Psi_\mu(R) = E_\mu(R)\Psi_\mu(R), \tag{2.3a}$$

with decaying boundary condition [20]. The complex eigenenergies are given by

$$E_\mu(R) = \mathrm{Re}\, E_\mu(R) - \frac{i}{2}\Gamma_\mu(R), \tag{2.3b}$$

where Γ_μ are the corresponding ionization rates. By $\mu = (n_1, n_2, m)$, where $n_1+n_2+|m|+1=n$, we denote the set of approximately good parabolic quantum numbers. That is, with the expression (2.2), and under the condition $\xi \ll \eta$, separating the variables in Eq. (2.3a) is possible in parabolic coordinates [20]. The proposed condition $\xi \ll \eta$ is well satisfied for high-eccentricity Rydberg states, i.e., the states with lower values for parabolic quantum number n_1 and with $m=0$, giving the main contribution to the ionization.

In the present paper we use the scaled parabolic coordinates $\tilde{\xi} = \xi/(2R\alpha)$ and $\tilde{\eta} = \eta/(2R\alpha)$, where α is a scaling parameter defined by

$$\alpha = \frac{-2E_\mu R}{Z - 1/4}. \tag{2.4}$$

Moreover, instead of $\tilde{\eta}$ we introduce the "effective" electron coordinate $u = \sqrt{\tilde{\eta}}$, which is technically a more convenient variable in the study of resonant electron transitions near the peak of the potential barrier [23]. Note that the u axis, like the $\tilde{\eta}$ and η axes, indicates the "direction" of most dominant electron transitions (see, for example, Fig. 2 in Ref. [20]). That is, along the u axis we have an infinite electron motion toward the surface; this property does not exist along the $\tilde{\xi}$ axis (where the electron motion is finite).

Accordingly, taking $\Psi_\mu = X_\mu(\tilde{\xi})Y_\mu(u)\exp(im\varphi)/(\sqrt{\xi}u)$, from Eq. (2.3a) we obtain the following differential equations with respect to the variables $\tilde{\xi}$ and u:

$$\frac{d^2X_\mu}{d\tilde{\xi}^2} + P^2(b, \lambda_\xi, \alpha; \tilde{\xi})X_\mu = 0, \tag{2.5a}$$

$$\frac{d^2Y_\mu}{du^2} + Q^2(b, \delta, \alpha; u)Y_\mu = 0. \tag{2.5b}$$

For P^2 and Q^2 we have $P^2 = -b^2/4 + b\lambda_\xi/\tilde{\xi} + (1-m^2)/(4\tilde{\xi}^2)$ and $Q^2 = b^2 h(u,d) - b\delta/(4d) + (1-4m^2)/(4u^2)$. The function $h(u,d)$ is given by

$$h = \frac{1}{4d} - u^2 + \frac{u^2(u^2 - \bar{u}^2)}{(1-\alpha u^2)(1-\alpha u^2/2)}, \tag{2.6}$$

where $\bar{u} = (Z-1/2)/[(Z-1/4)\alpha]$. The quantity d, introduced to equate the minimum and zero of the function $h(u,d)$, follows from the relations $h(u_0,d)=0$ and $h'(u_0,d)=0$.

The quantity b, defined by

$$b = 2(-2E_\mu)^{3/2}\frac{R^2}{Z-1/4}, \tag{2.7}$$

represents the large parameter for $R \approx R_c \gg 1$. The quantities λ_ξ and δ represent spectral parameters of Eqs. (2.5a) and (2.5b). Definition of the quantity δ is adapted to the vicinity of the effective potential barrier top in the u direction, i.e., we have

$$\delta = b - 16\lambda_\eta d, \tag{2.8a}$$

where λ_η is related to λ_ξ by the following equation:

$$(\lambda_\xi + \lambda_\eta)(-2E_\mu)^{1/2} = Z. \tag{2.8b}$$

B. The critical region of ionization, $R \approx R_c$

The details of solving the effective energy eigenvalue problems given by Eqs. (2.5a) and (2.5b), within the framework of the étalon equation method adapted to the critical region $R \approx R_c$, are given in Ref. [20]. Here we present the main features of the EEM in the case of highly charged ions $Z \gg 1$.

The basic idea underlying the EEM is in the fact that both Eqs. (2.5a) and (2.5b) represent equations of the form $y''(x) + p^2(b, \lambda; x)y(x) = 0$, with a large parameter b and a spectral parameter λ. The solution $y(x)$ and the values λ depend not only on the imposed boundary conditions, but also on the distribution of transition points (x_T) along the x axis, determined by $p^2(b, \lambda; x)$. For any configuration of the x_T points, a set of (partly overlapped) regions $\mathcal{A}_1$, $\mathcal{A}_2$,…. can be defined, so that transition points of neighboring regions are well separated. In the simplest cases it might be sufficient to use only one $\mathcal{A}$ region, containing all relevant transition points.

Determining the "local" solution $y_i(x)$, in the $\mathcal{A}_i$ region, by using the EEM, consists of choosing the appropriate étalon equation $\tilde{y}_i''(s_i) + \tilde{p}^2(b, \tilde{\lambda}_i; s_i)\tilde{y}_i(s_i) = 0$, where $s_i = s_i(x)$ and $\tilde{\lambda}_i$ are the new étalon variable and étalon spectral parameter, respectively. As mentioned in the Introduction, the étalon solution $\tilde{y}_i(s_i)$ must be exactly known, while the configuration of the étalon transition points s_{iT} must be compatible with that of the original equation in the $\mathcal{A}_i$ region, $s_{iT} = s_i(x_{iT})$. To relate $\tilde{y}_i(s_i)$ with $y_i(x)$ we set $y_i(x) = \tilde{y}_i(s_i)/\sqrt{s_i'}$, which leads us to a nonlinear differential equation for $s_i = s_i(x)$, i.e., we have $p^2(b, \lambda; x) - s_i'^2\tilde{p}^2(b, \tilde{\lambda}_i; s_i) - \{s_i, x\}/2 = 0$, where $\{s_i, x\} = s_i'''/s_i - 3s_i''^2/(2s_i')^2$ denotes the Schwartz derivative. The solution of this third-order equation follows from the expansion of $s_i(x)$ and λ into appropriate inverse power series with respect to b; as a consequence we get $y_i(x)$ and $\lambda = \lambda(\tilde{\lambda}_i)$ in the $\mathcal{A}_i$ region. Finally, we obtain the solution $y(x)$ and the spectral parameter λ by smooth matching of the asymptotic forms of $y_i(x)$ and by using relevant boundary conditions.

Along the $\tilde{\xi}$ axis, Eq. (2.5a) has two transition points for $m=0$; one pole $(\tilde{\xi}=0)$ and one turning point. For this simple case, it is sufficient to define only one region $\mathcal{A}$ encompassing these points, and use only one étalon equation of the Whittaker type. Following the standard EEM procedure [17] in the ion-surface interaction problem, we obtain the corresponding eigenfunction and effective energy, with spectral parameter λ_ξ given by

$$\lambda_\xi = n_1 + \frac{|m|+1}{2}. \tag{2.9}$$

Concerning Eq. (2.5b), the confluent turning points configuration, found on the u axis for $R \approx R_c^I$, compels us to use the EEM proposed in Ref. [20]. We consider two different regions along the u axis and use two appropriate étalon equations. In the vicinity of $u=0$, region $\mathcal{A}_1$, the étalon equation is a Bessel-type differential equation. The solution Y_1 is expressed via the Bessel function $J_m(w)$, where $w=w(u)$. In the region $\mathcal{A}_2$ that contains turning points $u_1 \approx u_2$, defined by $Q^2(u_{1,2})=0$, an appropriate étalon equation is the Weber differential equation

$$\frac{d^2U}{ds^2} + (s^2 - \epsilon)U = 0, \tag{2.10}$$

where $s=s(u)$ is the étalon variable and ϵ is the étalon spectral parameter for that region. Note that the parameter ϵ also represents a measure of the distance between turning points $s_1=-\sqrt{\epsilon}$ and $s_2=\sqrt{\epsilon}$ of Eq. (2.10). The confluence of these turning points corresponds to the $\epsilon=0$ condition.

For that reason, ϵ is a suitable parameter for the derivation of the critical distance R_c [20]. That is, by comparing the original equation (2.5b) with the étalon equation (2.10), we get $s_1=s(u_1)$ and $s_2=s(u_2)$, so that the equality $u_1=u_2$ is equivalent to $s_1=s_2$, i.e., the relation $\epsilon=0$ holds. Taking into account that the confluence of the turning points u_1 and u_2 occurs at critical distance R_c, we get the condition

$$\mathrm{Re}\ \epsilon(R_c) = 0. \tag{2.11}$$

The general solution $U(s)$ of Eq. (2.10) is a linear combination of the parabolic cylinder functions. The solution Y_2 of Eq. (2.5b) in the considered region is given by $Y_2 = U(s)/\sqrt{s'}$, where $s'=ds/du$. By using the étalon equation method we obtain the function $s=s(u)$ in the form of appropriate asymptotic series. This approach requires that the condition $\delta=\kappa\epsilon$, where $\kappa=2\sqrt{2h''(u_0)}d$, is satisfied. The proportionality of parameters δ and ϵ indicates that $\mathrm{Re}\ \delta(R_c)=0$.

The quantity $\epsilon(R)=s^2(u_1)$ is positive for $R>R_c$ and negative for $R<R_c$. Therefore, in the region $R>R_c$ we have the real turning points $s_{1,2}=\mp\sqrt{\epsilon}$, i.e., the corresponding electron transitions are of the subbarrier type. On the other hand, for $R<R_c$ we have $\epsilon<0$ so that the turning points $s_{1,2}$ are complex $(s_{1,2}=\mp i\sqrt{|\epsilon|})$; the corresponding electron transitions are overbarrier in character.

This is a key technical detail of the EEM, not available in other existing nonperturbative methods. In other words, for $R>R_c$ we have the subbarrier transitions while for $R<R_c$ the electron transitions are overbarrier. This "overbarrier-subbarrier rule" will be useful for interpreting relevant graphs in Sec. III. We point out that the electron transitions (from the ionic region toward the solid) are energetically possible only for $R<R_F$, where Fermi distance R_F is defined by

$$\mathrm{Re}\ E_\mu(R_F) = -\phi. \tag{2.12}$$

By ϕ we denote the solid work function.

The functions $Y_1(u)$ and $Y_2(u)$ must be smoothly matched in the region $\mathcal{A}_1 \cap \mathcal{A}_2$. By using the asymptotic forms of the solutions Y_1 and Y_2, and taking into account the outgoing wave behavior of $Y_2(u)$ for $u \gg u_2$, from the matching condition $Y_1/Y_1' = Y_2/Y_2'$, we obtain the following system of algebraic equations for the quantities $\Gamma_\mu(R)$, $\mathrm{Re}\ E_\mu(R)$, and $\mathrm{Re}\ \epsilon(R)$ [Eqs. (3.10a)–(3.10c) in Ref. [20]):

$$\mathrm{Re}\ \epsilon = \frac{f_1\ \mathrm{Re}\ b + 2\pi(2n_2+m+1)}{f_2 - \ln(\mathrm{Re}\ b)}\left[1 + O\left(\frac{1}{b}\right)\right], \tag{2.13a}$$

$$\Gamma_\mu = \frac{-2\ \mathrm{Re}\ E_\mu}{\mathrm{Re}\ b} \times \frac{\ln[1+\exp(-\pi\ \mathrm{Re}\ \epsilon)]}{[\ln(\mathrm{Re}\ b) - f_2](a_1 + a_2/\mathrm{Re}\ b) + f_3 + O(\ln b/b^2)}, \tag{2.13b}$$

$$\mathrm{Re}\ E_\mu = -\frac{Z^2}{2}\left[\lambda_\xi + \frac{\mathrm{Re}\ b}{16\ \mathrm{Re}\ d} - a_3\ \mathrm{Re}\ \epsilon + O\left(\frac{1}{b^2}\right)\right]^{-2}. \tag{2.13c}$$

The quantities $\mathrm{Re}\ b$ and λ_ξ figuring in Eqs. (2.13a), (2.13b), and (2.13c) are given by Eqs. (2.7) and (2.9), respectively. The analytic expressions of a_1, a_2, and a_3 introduced in Eqs. (2.13b) and (2.13c), as well as the functions f_1, f_2, and f_3, are given explicitly in the Appendix of Ref. [20], taking into account that in the present case $\tilde{F}=0$.

The system of equations (2.13a), (2.13b), and (2.13c) for $\mathrm{Re}\ \epsilon$, Γ_μ, and $\mathrm{Re}\ E_\mu$ may seem complicated due to additional interrelated R-dependent quantities, but has a relatively simple structure: $\mathrm{Re}\ \epsilon = \mathcal{F}_1(\mathrm{Re}\ E_\mu)$, $\Gamma_\mu = \mathcal{F}_2(\mathrm{Re}\ \epsilon, \mathrm{Re}\ E_\mu)$, and $\mathrm{Re}\ E_\mu = \mathcal{F}_3(\mathcal{F}_1(\mathrm{Re}\ E_\mu), \mathrm{Re}\ E_\mu)$, where $\mathcal{F}_1$, $\mathcal{F}_2$, and $\mathcal{F}_3$ represent known nonlinear functions of the variables indicated. Accordingly, the numerical treatment of the system is straightforward; for details see Ref. [20], Sec. III B. Due to the structure of Eqs. (2.13a), (2.13b), and (2.13c) the quantities $\mathrm{Re}\ \epsilon(R)$, $\Gamma_\mu(R)$, and $\mathrm{Re}\ E_\mu(R)$ must be determined simultaneously; this is characteristic for the EEM when solving the quasistationary eigenvalue problem for $R \approx R_c$.

From the analysis presented we see that the critical distance R_c, Eq. (2.11), plays a role somewhat similar to that of the distance R_c^{class} used in the COB model [1]. Indeed, both quantities describe a situation when the energy level is at the top of a potential barrier, regardless of the direction of electronic transitions inside the ion-surface system. Nevertheless, the concept of R_c differs from R_c^{class}, at least for the following reasons. We recall that the R_c^{class} follows from identifying the value of the potential barrier top $U(z_m,R)$ on the z axis with a simple expression for the energy level $E_n(R)$; consequently, R_c^{class} depends exclusively on the quantum number n and the ionic core charge Z. On the other hand, the distance R_c proposed by the EEM is essentially associated with the effective potential barrier along the u direction and the effective energy, Eq. (2.5b). Therefore, the R_c values follow from a full quantum treatment of the complex energy eigenvalue prob-

lem in the parabolic coordinates, i.e., from the system of coupled equations (2.13a), (2.13b), and (2.13c), so that $R_c = R_c(n_1, n_2, m; Z)$.

The overbarrier-subbarrier rule of the ionization dynamics was introduced above on rather formal grounds, i.e., we analyzed the R dependence of the quasimomentum Q^2 of Eq. (2.5b) and the corresponding étalon quasimomentum $\tilde{Q}^2 = s^2 - \epsilon$ of Eq. (2.10). The behavior of these quasimomenta can also be expressed in terms of the effective potential and effective energy of Eq. (2.5b). In that sense, the overbarrier-subbarrier rule reflects the following physically more transparent fact: during the ionic motion toward the surface, the effective energy level lifts (simultaneously with the decreasing of the effective barrier), so that below a certain value of the distance R, the overbarrier transitions become possible.

C. Rate equation and the ionization distance R_c^I

The results exposed in Secs. II A and II B, corresponding to relatively detailed summaries of Secs. II and III of Ref. [20], represent a basis for identifying the critical region of ionization $R \approx R_c$ of a multiply charged ionic projectile. We recall that in Ref. [20] we considered the ionization distances R_c^I of hyperthermal neutral atoms ($Z=1$) approaching the surface with constant velocity $v_\perp$. For the purpose of the present paper, however, we need an additional analysis which will take into account the acceleration of the projectile $Z \gg 1$ under the influence of a polarized metal surface. Our main task is to elaborate on the concept of the ionization distance R_c^I for these projectiles.

In order to define the ionization distance $R_c^I(n)$ of moving ions with $Z \gg 1$, it is necessary to obtain the ionization probability $P_\mu(R)$. We consider the quantity $P_\mu(R)$ in the adiabatic approximation of decaying states (see Sec. II A) by using an approximate rate equation approach and the supposition of the classical law of ionic motion.

Generally, the problem of ionization of one-electron multiply charged Rydberg ions approaching solid surfaces would require a multichannel model, which includes both resonant ionizations and neutralizations, as well as Auger and radiative processes. Also, in the energy-term crossing region, the transitions between different adiabatic decaying states Ψ_μ could be relevant. In this form, the accurate solution of the problem is not yet known. However, by using some physically plausible approximations, for the R_c^I problem treated in the present paper, it is possible to estimate the contribution of these additional channels, opened simultaneously with the ionization one.

Our analysis is based on the concept of critical value of principal quantum number n_c, defined as an integer solution of the equation

$$R_c(n_c) = R_F(n_c). \tag{2.14}$$

It turns out that, during the ionic motion toward the surface from $R=\infty$ to $R=R_c^I(n)$, the resonant ionization of the occupied Rydberg state $n \geqslant n_c$ is a dominant process. The resonant neutralizations of empty Rydberg states of the same traveling ion are practically negligible. These conclusions follow from an analysis of relevant graphs for the energy terms and corresponding rates, which will be explicated in Sec. III A. Also, the behavior of the energy terms and ionization rates of two neighboring energy manifolds indicates that the electron transitions between adiabatic decaying states Ψ_μ can be neglected for lower values of the first parabolic quantum number n_1 and for $m=0$.

The contribution of radiative deexcitation of the $Z \gg 1$ ion, with the occupied one-electron state $n \geqslant n_c$, can be neglected during the ionic motion toward the solid surface, because the radiative processes are significantly slower than the ionization process. The Auger processes can also be neglected in the considered ionization; namely, as two-electron nonresonant processes, the Auger neutralization or ionization require an internal energy conversion, meaning that they are localized closer to the surface in comparison to the distance $R_c^I(n)$ [25].

Therefore, for $n \geqslant n_c$ the system of coupled rate equations is reduced to a simple rate equation if the n_1 values are not too high, $m=0$, and $R < R_F(n)$. The ionization probability $P_\mu(R)$ of the occupied electronic state $\mu=(n_1, n_2, m)$ is given by

$$v_\perp(R)\frac{dP_\mu(R)}{dR} = -\Gamma_\mu(1 - P_\mu(R)), \tag{2.15}$$

where $v_\perp(R) = -dR/dt$ represents the perpendicular ionic velocity at the ion-surface distance R. Note that Eq. (2.15) is not adequate for the empty states $n < n_c$, where the multichannel processes determine the stepwise neutralization dynamics. We also assume that the ionic projectile with core charge $Z \gg 1$ and mass M approaches the solid surface according to the classical energy conservation law:

$$\frac{1}{2}Mv_{\perp 0}^2 = \frac{1}{2}Mv_\perp^2(R) + W(R, v_\perp), \tag{2.16}$$

where $v_{\perp 0} = v_\perp(\infty)$ is the initial perpendicular ionic velocity. The quantity W in Eq. (2.16) is the potential energy of the ion at a distance R from the surface.

As in the case of stepwise neutralization dynamics [26], the "true" potential energy W of multiply charged ion impinging on the solid surface depends on the solid response. Since the ionization distances R_c^I are larger than those characteristic for the nonlinear effects, the response is mainly linear. Accordingly, in Eq. (2.16) we take

$$W(R, v_\perp) = W_{cl}(R) f(R, v_\perp), \tag{2.17a}$$

where $W_{cl} = -Z^2/(4R)$ is the classical potential energy of interaction of the charge Z with its image. Using the dielectric response theory and surface plasmon pole approximation, see Ref. [1] and references therein, the factor f is given by the following expression:

$$f(R, v_\perp) = \int_0^\infty \frac{e^{-x}}{1 + g(x/R, v_\perp)} dx, \tag{2.17b}$$

where $g \approx g_1 x/R + g_2(g_3 + v^2)(x/R)^2$. By estimating the numerical values of parameters g_1, g_2, and g_3, we conclude that for $Z \gg 1$, $n \geqslant n_c$ and for $R \approx R_c$, $v \leqslant 1$ a.u., the contribution of the function g in the integral (2.17b) is negligible, so that

$f \approx 1$. Therefore, the dynamical response of the surface reduces to the classical image forces: $W \approx W_{cl}$, i.e., we have the classical image acceleration of the ion.

According to Eq. (2.16), for the velocity $v_\perp = v_\perp(R)$, we get

$$v_\perp^2(R) = v_{\perp 0}^2 + \frac{Z^2}{2MR}. \tag{2.18}$$

We point out that the simple estimation of the condition of validity of Eq. (2.18) can be expressed as $R \gg R_{sc}$, where $R_{sc} = v_F / w_s$ is the screening length, whereas v_F is the Fermi velocity and $w_s = \sqrt{2} w_p$ is the surface plasmon frequency.

Under the conditions mentioned, from Eq. (2.15) together with the condition $P_\mu(R_F) = 0$, for $R < R_F$ we get

$$P_\mu(R) = 1 - \exp\left(- \int_R^{R_F} \frac{\Gamma_\mu(R)}{v_\perp(R)} dR \right). \tag{2.19}$$

We define the ionization distance $R_c^I(\mu, Z, v_{\perp 0})$ as a maximum of the total ionization rate $\tilde{\Gamma}_\mu(R) = dP_\mu/dt = -v_\perp(R) dP_\mu(R)/dR$, i.e., we have

$$\left(\frac{d\tilde{\Gamma}_\mu}{dR} \right)_{R_c^I} = 0. \tag{2.20a}$$

A simple argument supports the existence of the peak of $\tilde{\Gamma}_\mu(R)$ at some $R = R_c^I$, despite the fact that the ionization rate $\Gamma_\mu(R)$ will be a strongly decreasing function of increasing R; see, for example, Figs. 1(a), 2(a), and 3(a). That is, from Eq. (2.15) we see that $\tilde{\Gamma}_\mu(R)$ represents a product of $\Gamma_\mu(R)$ and an increasing survival probability $1 - P_\mu(R)$; see Figs. 4(a), 5(a), and 6(a). This produces a strongly peaked total ionization rate $\tilde{\Gamma}_\mu(R)$ in the critical region $R \approx R_c$.

Using Eqs. (2.15) and (2.19), the definition (2.20a) can be rewritten in a more practical form,

$$\left(\frac{d\Gamma_\mu}{dR} \right)_{R_c^I} + \frac{1}{v_\perp(R_c^I)} \Gamma_\mu^2(R_c^I) = 0. \tag{2.20b}$$

From Eq. (2.20b) we see that the distance R_c^I, in contrast to the R_c distance, represents a velocity-dependent quantity. In our subsequent considerations (Sec. III C), by direct numerical treatment we shall expose that $R_c^I = f(v_{\perp 0}) R_c$, and that R_c^I is close to R_c; in other words, the resonant ionization takes place in the very vicinity of the effective potential barrier top along the u direction.

III. IONIZATION OF THE MULTIPLY CHARGED RYDBERG IONS

A. The eigenenergies and rates $\mathrm{Re}\, E_\mu(R)$ and $\Gamma_\mu(R)$

Using the expressions (2.13a), (2.13b), and (2.13c), we calculate the ionization rates and energies, characteristic for the ionization dynamics in the critical region $R \approx R_c$.

In Fig. 1 we present the ionization rates $\Gamma_\mu(R)$ and energy terms $\mathrm{Re}\, E_\mu(R)$ for $Z=8$ and $n = 9, 10, \ldots, 14$, for $n_1 = 0$ and $m = 0$, relevant for comparison with the CAM method [7]. In order to illustrate the overbarrier-subbarrier rule (see Sec. II B), the R_c symbols (◦) are connected by appropriate thin lines. The numerical values of the critical distance R_c are obtained on the basis of Eq. (2.11).

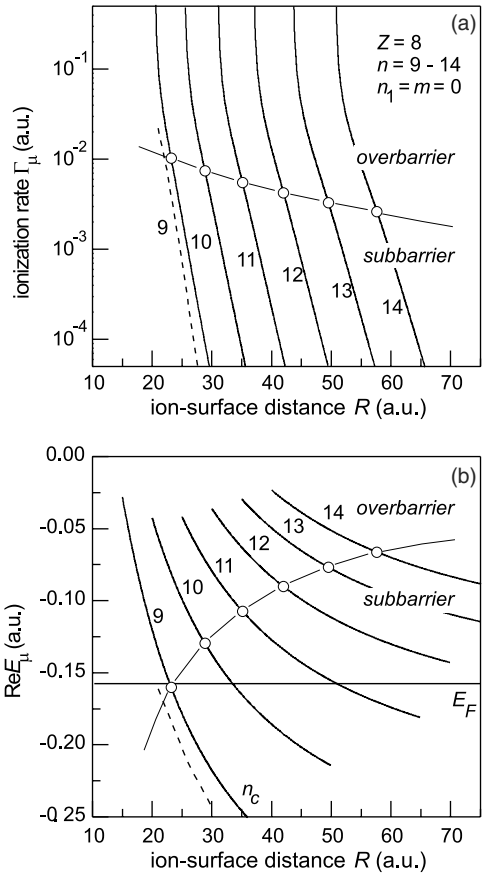

FIG. 1. Ionization of multiply charged O^{7+} ($Z=8$) ions in the Rydberg states $n = 9, 10, \ldots, 14$, $n_1 = 0$, and $m = 0$: (a) ionization rates $\Gamma_\mu(R)$ and (b) energies $\mathrm{Re}\, E_\mu(R)$. The dashed curves are the CAM method results [7] for $n=9$. Circles indicate the positions of critical distances R_c. By E_F we denote the Fermi level of the Al solid with work function $\phi = 4.29$ eV $= 0.16$ a.u. Intersections of the curves presented in Fig. 1(b) with E_F indicate the Fermi distances R_F.

From Fig. 1 we recognize some features of the ionization process in the critical regions; namely, the EEM ionization rates in Fig. 1(a) are characterized by the vertical asymptotes in the overbarrier region ($R < R_c$) with exponentially decreasing behavior in the vicinity of $R \approx R_c$. The curves corresponding to higher n are positioned at larger ion-surface distances R. The energy terms presented in Fig. 1(b) show monotonically increasing behavior with the decrease of R. For $n=9$ the rate and energy term follow the available results of the CAM method [7], the dashed curves in Fig. 1. Taking into account that $R_c \approx R_c^I$, for sufficiently slow ions (see Sec. III C), we conclude that those occupied states with $n < n_c = 9$ cannot be resonantly ionized, $\mathrm{Re}\, E_\mu(R_c) < -\phi$. The ionization of the $Z=8$ ion is possible exclusively for the states with $n \geq 9$.

Using the information in Figs. 1(a) and 1(b) it is possible to estimate the contribution of neutralization channels, which

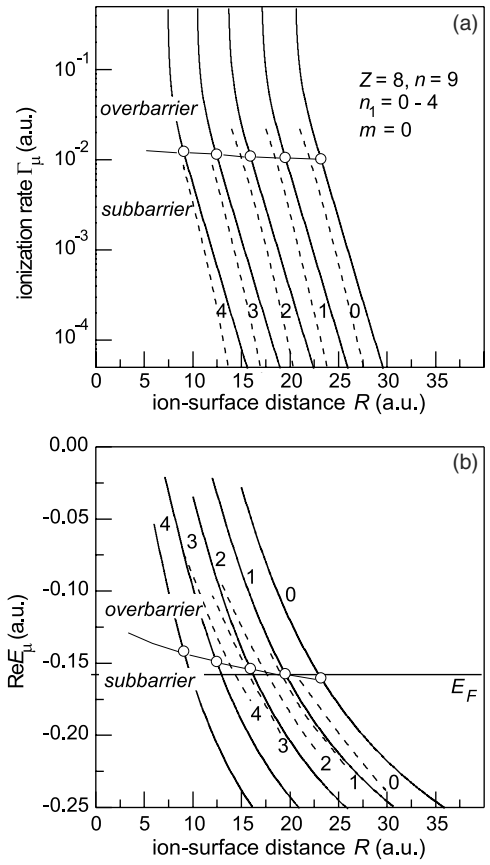

FIG. 2. (a) Ionization rates $\Gamma_\mu(R)$ of multiply charged ions with core charge $Z=8$ in the Rydberg states $n=9$, $n_1=0-4$, and $m=0$ (full curves), and (b) the corresponding energy manifold. The dashed curves are the CAM method results [7] for $n=9$. Circles indicate the positions of critical distances R_c. By E_F we denote the Fermi level of the Al solid.

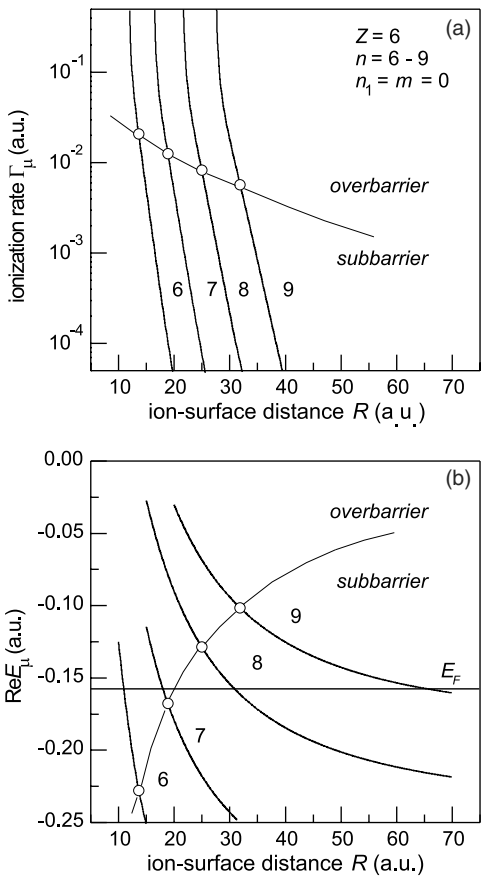

FIG. 3. Ionization of Ar^{5+} and subsequent neutralization of Ar^{6+} multiply charged ($Z=6$) ions in the Rydberg states $n=6$, 7, 8, and 9, $n_1=0$, and $m=0$: (a) ionization rates $\Gamma_\mu(R)$ and (b) energies $\mathrm{Re}\,E_\mu(R)$. Circles indicate the positions of critical distances R_c. By E_F we denote the Fermi level of the Al solid.

might be open simultaneously with the ionization channel. That is, when the one-electron Rydberg ion $Z=8$ approaches a solid surface, together with a given occupied state $n \geqslant n_c$ there also travels a set of empty states [which could be populated with some rate $\Gamma_\mu^N(R)$ by a resonant neutralization mechanism]. Determining the corresponding rates $\Gamma_\mu^N(R)$ is a separate problem [16,17,19] not discussed in the present EEM decay model, because the evolution of the state Ψ_μ is not a time-reversal process. However, the resonant ionization and neutralization processes are interrelated by an asymptotically accurate "detailed balance principle" [27]. Accordingly, the rates $\Gamma_\mu^N(R)$ can be estimated using the EEM rates $\Gamma_\mu(R)$ for $\mathrm{Re}\,E_\mu(R)<E_F$, i.e., we can "read" the values of the electron capture rates directly from Fig. 1(a).

To clarify, we choose the $n=12$ occupied electronic state and classify the empty states of the same ion into three groups: $n'>12$, $9<n''<12$, and $n'''\leqslant 9$. In principle, the states $n'>12$ can be populated by a resonant neutralization process for $\mathrm{Re}\,E_\mu<E_F$; however, this process would be either energetically impossible, or possible at very large ion-surface distances R with a practically negligible probability. The lower empty states $9<n''<12$ of the same ion can be resonantly populated at smaller ion-surface distances, but likewise with a vanishing probability [for example, for $n=10$ from Fig. 1(a) we see that the rate Γ_μ is smaller than 10^{-4} a.u.]. Finally, the empty states $n'''\leqslant 9$ can be neutralized, but only after the ionization of the considered Rydberg state $n=12$ is almost completed; for that reason, these neutralization channels can also be neglected. Accordingly, when the ion $Z=8$ with filled electronic state $n=12\geqslant n_c=9$ approaches the Al surface, the contribution of all neutralization channels is practically negligible. A similar analysis can also be performed for occupied electronic states $n\neq 12$ in Fig. 1.

In Fig. 2 we expose the ionization rates and energies for $Z=8$, $n=9$, $m=0$, and for the first parabolic quantum number $n_1=0$, 1, 2, 3, and 4. A general agreement with the CAM method results (dashed curves) is obtained for all considered values of n_1, especially for the rates Γ_μ around the critical distances R_c [see Fig. 2(a)]. This is a significant fact because the presented EEM and CAM approaches are very different nonperturbative methods. Since the EEM rates correspond to the high-eccentricity ("low-n_1") Rydberg states, a full agreement with the rates (and energies) obtained by the CAM method [7] is not possible (see Sec. IV). The difference between the EEM and CAM method energy curves, evident in Fig. 2(b) for higher n_1 values, suggests that the higher-l terms in the CAM model [7] scattering wave function begin to be relevant.

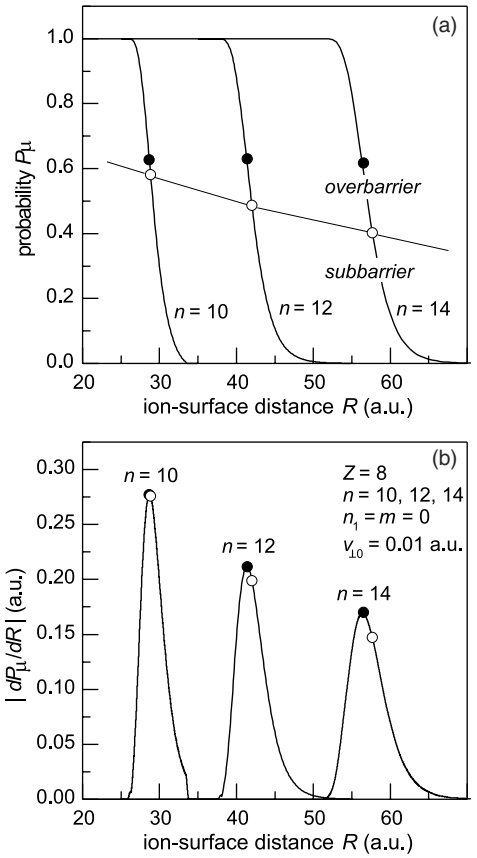

FIG. 4. The n dependence of (a) the ionization probability $P_\mu(R)$ and (b) the quantity $|dP_\mu/dR|$ for Rydberg states $n=10$, 12, and 14, $n_1=0$, and $m=0$ of O^{7+} ($Z=8, M=2ZM_p$) ion. The initial perpendicular ionic velocity is $v_{\perp 0}=0.01$ a.u. Dots and circles indicate the positions of ionization distances R_c^I and critical distances R_c, respectively.

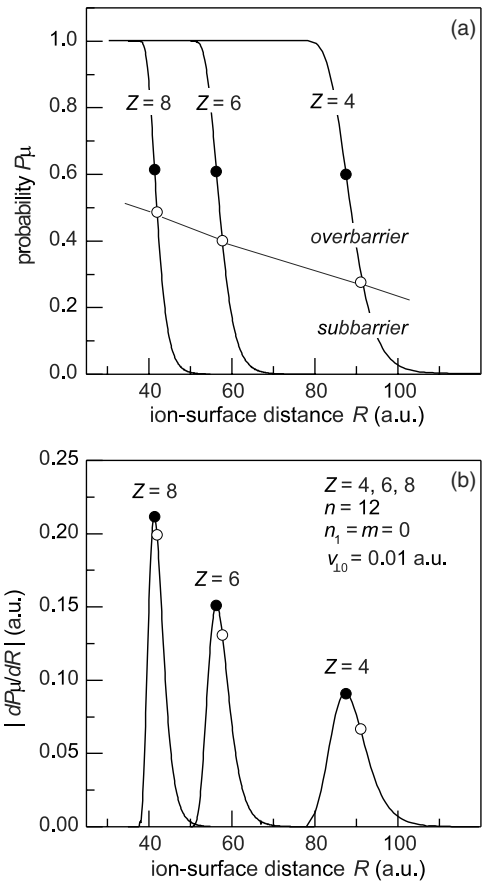

FIG. 5. The Z dependence of (a) the ionization probability $P_\mu(R)$ of the Rydberg state $n=12$, $n_1=m=0$, for $Z=4$, 6, and 8 ($M=2ZM_p$) with $v_{\perp 0}=0.01$ a.u., and (b) the quantity $|dP_\mu/dR|$. Dots and circles indicate the positions of ionization distances R_c^I and critical distances R_c, respectively.

Graphs similar to those for the manifold $n=9$ in Fig. 2 can also be presented for higher n manifolds ($n=10, 11, 12, \ldots$). It turns out that some energy terms of two neighboring manifolds intersect. By analyzing energy terms and rates as in the analysis presented above, we can estimate the contribution of the "crossing region" to resonant ionization of a given occupied electronic state. To do this, we define the ionic position $R=R^*$ where an occupied electronic term $\mathrm{Re}\, E_{\mu_1}$ intersects a neighboring empty term $\mathrm{Re}\, E_{\mu_2}$. This estimation is based on the fact that these terms have rather different ionization distances $R_{c,1}^I$ and $R_{c,2}^I$.

Our analysis shows that the lower-n_1 term $\mathrm{Re}\, E_{\mu_1}$ (for example, the term with $n=11$ and $n_1=0$), being previously occupied, intersects the larger-n_1 empty term $\mathrm{Re}\, E_{\mu_2}$ (with $n=12$ and $n_1=4$) at $R=R^\star$ (where $R^\star \approx 52$ a.u. in the example considered). For $R<R^\star$ the subsequent time evolution of the occupied electronic state Ψ_{μ_1} can continue either along the energy term $\mathrm{Re}\, E_{\mu_1}$ or along the previously empty term $\mathrm{Re}\, E_{\mu_2}$, continuing its evolution in the state Ψ_{μ_2}. Both of these states decay, so that the alternative state evolutions end with resonant ionizations, but at different ionization distances $R_{c,1}^I > R_{c,2}^I$; namely, $R_{c,1}^I = 35.1$ a.u. and $R_{c,2}^I = 22.8$ a.u. Therefore, the ionization of the larger-n_1 state Ψ_{μ_2} could take place at the time when the ionization of the lower-n_1 state Ψ_{μ_1} is practically finished. Accordingly, the electron transition $\Psi_{\mu_1} \to \Psi_{\mu_2}$ does not play a decisive role in the resonant ionization of the low-n_1 occupied states. Extending these conclusions to the ionization of large-n_1 Rydberg states is not possible within the framework of EEM approach presented in this paper (see Sec. IV).

In Fig. 3 we present the case of ion $Z=6$, relevant for comparing the EEM predictions to the classical overbarrier model results [28]. The ionization rates and energies of one-electron Rydberg states with $n=6$, 7, 8, and 9 and $n_1=m=0$ are presented. For the critical values of n_c one obtains $n_c=8$, corresponding to $R_c(8)=25.2$ a.u., whereas for $n=7<n_c$ we get $R_c(7)=19.3$ a.u. Note that the energy level positions at these ion-surface distances are above and below the Fermi level E_F of the Al target, respectively [Fig. 3(b)]. Accordingly, the occupied level $n=8$ is the lowest one that can be resonantly ionized. On the other hand, if the level $n=7$ should be empty it would be the highest one that can be resonantly populated, meaning that $R_c(7)$ corresponds to the first neutralization distance: $R_1^N(n) \approx R_c(7)$.

These conclusions are compatible with the estimation for the first neutralization distance ($R_1^N \approx 22$ a.u.) obtained within the framework of the COB model [28] for Ar^{6+} slowly

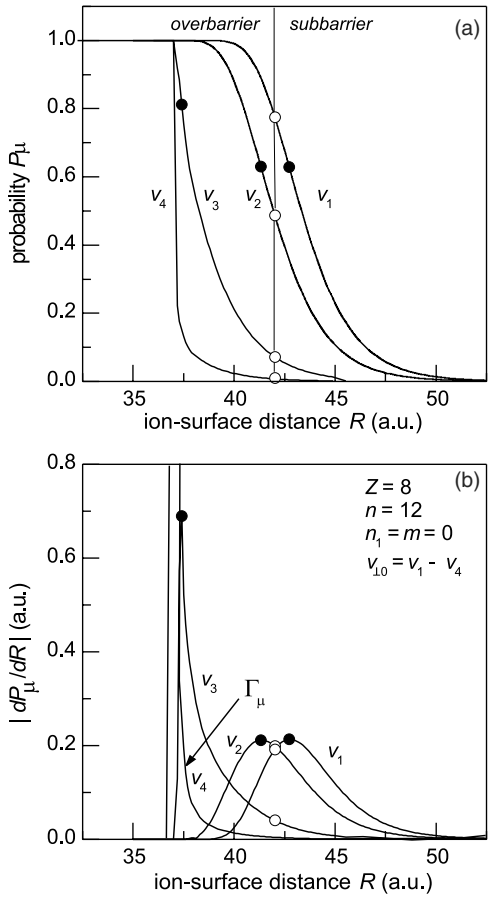

FIG. 6. The $v_{\perp 0}$ dependence of (a) the ionization probability $P_\mu(R)$ and (b) the quantity $|dP_\mu/dR|$ for the Rydberg state $n=12$, $n_1=0$, and $m=0$ of O^{7+} ($Z=8, M=2ZM_p$) ion. The initial ionic velocities $v_{\perp 0}$ are $v_1=0.000\,01$ a.u., $v_2=0.01$ a.u., $v_3=0.1$ a.u., and $v_4=1$ a.u. Dots and circles indicate the positions of ionization distances R_c^I and critical distances R_c, respectively.

approaching the Al surface; namely, in the charge state evolution, the ionization of the initial ion Ar^{5+}, directed toward the Al surface, precedes the first neutralization of the formed ion Ar^{6+}. In that sense, the ionization problem of the ion Ar^{5+} is a complement of the first neutralization distance problem of the Ar^{6+} ion (discussed within the analysis [28] of image acceleration effect during the stepwise neutralization cascade). In other words, the change of direction of the electron current in the considered ion-surface system takes place in the narrow region $\Delta R \approx 5$ a.u. of the R distance around the value $R \approx R_1^N \approx 22$ a.u.

B. The ionization probability $P_\mu(R)$ and total rate $\tilde{\Gamma}_\mu(R)$

The intermediate stages of the ionization process are characterized by the ionization probability $P_\mu(R)$, Eq. (2.19), and the total ionization rate $\tilde{\Gamma}(R)=dP_\mu/dt=v_\perp|dP_\mu/dR|$.

In Fig. 4(a) we present the n dependence of ionization probabilities $P_\mu(R)$ for the O^{7+} ion with core charge $Z=8$ and mass $M=16M_p$, where $M_p=1836$ is the mass of the nucleon, approaching the Al solid surface. For the initial perpendicular ionic velocity we take $v_{\perp 0}=0.01$ a.u. We consider the Rydberg states $n=10$, 12, and 14, $n_1=m=0$, satisfying the condition $n \geqslant n_c=9$. In Fig. 4(b) we present the quantity $|dP_\mu/dR|$. The Fermi distances R_F, figuring in Eq. (2.19) for $P_\mu(R)$, are given by $R_F(10)=33.5$, $R_F(12)=87.0$, and $R_F(14)=364.0$ (in atomic units).

From Fig. 4(a) we see that the considered Rydberg states will be completely ionized $[P_\mu(R)\to 1]$ at a finite ion-surface distance R. The quantity $|dP_\mu(R)/dR|$ presented in Fig. 4(b) exhibits maxima which determine the ionization distances R_c^I (dots in Fig. 4). The corresponding ionization distances R_c^I increase with the increase of n; this trend is followed by a mild increase of $|R_c^I-R_c|$. According to Fig. 4(a) we can estimate the contributions of the overbarrier and subbarrier electron transitions. We see that the contribution of the overbarrier transitions increases with the increasing of n.

In Fig. 5(a) we expose the Z dependence of the ionization probability $P_\mu(R)$ for $Z=4$, 6, and 8 and $M=2ZM_p$ for $n=12$ and $n_1=m=0$, considering the case $v_{\perp 0}=0.01$ a.u. The critical distances R_c and ionization distances R_c^I are marked by circles and dots, respectively. The sequence of the corresponding $|dP_\mu/dR|$ curves is presented in Fig. 5(b). The Fermi distance for $Z=8$ is $R_F=87.0$ a.u.; the R_F values for $Z=4$ and 6 are very large, $R_F>500$ a.u. From Fig. 5(a) we see that the considered Rydberg states will also be completely ionized at a finite ion-surface distance R. The ionization distances, as well as the critical distances, decrease with the increasing of Z. The quantity $|R_c^I-R_c|$ decreases slightly with the increasing of Z.

In Fig. 6(a) we present the velocity dependence of the ionization probabilities $P_\mu(R)$ for the O^{7+} ion ($Z=8$) in the Rydberg state $n=12$, $n_1=m=0$. The curves correspond to four different initial ionic velocities (values are given in the figure caption). The Fermi distance for the considered case is $R_F=870$ a.u. In Fig. 6(b) we present the quantity $|dP_\mu/dR|$.

From Fig. 6 we see that the ionization distances R_c^I decrease with the increasing of $v_{\perp 0}$. The relative positions of the ionization distances R_c^I and critical distances R_c also depend on the ionic velocity $v_{\perp 0}$. For $v_{\perp 0} \equiv v_1=0.000\,01$ a.u. we have $R_c^I > R_c$, whereas for $v_{\perp 0} \gtrsim 0.01$ a.u. we have $R_c^I < R_c$. In the first case the ionization mechanism is mainly a tunneling one (80% tunneling, 20% overbarrier); the case $v_{\perp 0} \equiv v_2=0.01$ a.u. corresponds to an equal contribution of these two aspects of the electron exchange mechanism. In the case $v_{\perp 0} \equiv v_3=0.1$ a.u. the tunneling contribution is negligible (5%) and the case $v_{\perp 0} \equiv v_4=1$ a.u. corresponds to a completely overbarrier electron transition.

Also, from Fig. 6 we see that the considered Rydberg states will be ionized with different dynamics for different $v_{\perp 0}$; namely, the quantities $|dP_\mu(R)/dR|$ for $v_{\perp 0} \leqslant 0.01$ a.u. represent bell-shaped curves with widths $\delta R \approx 5$ a.u.; these curves become very sharp ($\delta R \to 0$) for the ionic velocities $v_{\perp 0} \approx 1$ a.u. Consequently, the "ionization mean time" $\delta t = \delta R / v_\perp(R_c^I)$ of the traveling ion becomes very short in the limiting intermediate-velocity region.

An additional specific feature of the ionization of multiply charged ions can be recognized from Fig. 6; namely, in the low-velocity case the ionization is governed by a total bell-shaped ionization rate $\tilde{\Gamma}_\mu(R)$. On the other hand, the ionization at intermediate velocities ($v_{\perp 0} \equiv v_4 \approx 1$ a.u.) can be de-

TABLE I. The critical distances R_c, Fermi distances R_F, and ionization distances $R_c^I(v_{\perp 0})$ (in a.u.). The relevant cases of Rydberg states $(n,n_1=0,m=0)$ of multiply charged ions (core charges Z, $M=2ZM_p$) approaching an Al solid surface are presented. For the initial ionic velocities $v_{\perp 0}$ we take $v_1=0.000\,01$ a.u., $v_2=0.01$ a.u., $v_3=0.1$ a.u., and $v_4=1$ a.u. The velocity-independent EEM values of R_c^I, taken from Ref. [18], as well as COB values R_c^{class} according to Ref. [1], are also presented.

		n				
		10	11	12	13	14
$Z=6$	R_c	39.6	48.3	57.7	68.1	79.2
	R_F	318.4	433.3			
	$R_c^I(v_1)$	40.6	49.2	59.5	68.7	79.9
	$R_c^I(v_2)$	39.4	47.0	56.1	66.0	76.9
	$R_c^I(v_3)$	35.8	42.8	51.9	61.1	71.0
	$R_c^I(v_4)$	34.2	41.5	49.6	58.4	67.8
[18]	R_c^I	34.5	41.9	49.7	58.3	67.7
[1]	R_c^{class}	34.5	41.8	49.7	58.3	67.7
$Z=7$	R_c	33.4	40.7	48.7	57.4	66.8
	R_F	54.0	129.9	346.52		
	$R_c^I(v_1)$	34.4	41.5	49.5	58.3	67.6
	$R_c^I(v_2)$	32.8	39.9	47.5	56.0	65.2
	$R_c^I(v_3)$	30.5	37.0	44.2	58.0	60.4
	$R_c^I(v_4)$	29.3	35.6	42.6	50.1	58.2
[18]	R_c^I	29.6	35.9	42.6	50.0	58.0
[1]	R_c^{class}	28.5	34.5	41.1	48.2	55.9
$Z=8$	R_c	28.8	35.1	42.0	49.5	57.7
	R_F	33.5	51.0	87.0	199.7	364.0
	$R_c^I(v_1)$	29.6	35.8	42.7	50.2	58.3
	$R_c^I(v_2)$	28.7	34.7	41.3	48.5	56.6
	$R_c^I(v_3)$	26.6	32.2	38.4	45.2	52.6
	$R_c^I(v_4)$	25.7	31.2	37.3	43.9	51.0
[18]	R_c^I	25.9	31.4	37.3	43.7	50.7
[1]	R_c^{class}	24.2	29.3	34.9	40.9	47.5

scribed by the rates $\Gamma_\mu(R)$, representing a monotonically increasing function with decreasing R (with a vertical asymptote); see Fig. 6(b). This fact has been used in our previous analysis of the population-reionization process of multiply charged ions escaping solid surface with intermediate velocities [18].

C. The critical and ionization distances R_c and R_c^I

The most important output of our calculations concerns the ionization distances R_c^I which provide us with basic physical information about the ionization process. In the EEM presented, the ionization distances depend on the parabolic quantum numbers n_1, n_2, and m. In addition, the values of R_c^I depend on the ionic core charge Z and mass M, as well as the ionic perpendicular velocity $v_{\perp 0}$.

In Table I we present the R_c, R_F, and R_c^I numerical values (in atomic units), calculated by Eqs. (2.11), (2.12), and (2.20b), respectively, for $n=10,\ldots,14$, $n_1=0$, and $m=0$, with core charges $Z=6$, 7, and 8 (and masses $M=2ZM_p$), for ions approaching the Al solid surface. The initial perpendicular ionic velocities $v_{\perp 0}$ are given in the table caption. The R_F values not indicated in Table I are very large. In the same table we present the EEM ionization distances taken from Ref. [18], which are independent of projectile velocities. Also, we present the COB values R_c^{class} according to Ref. [1].

The R_c^I trends we see in Table I can be summarized as follows. For fixed Z and $v_{\perp 0}$, the distance R_c^I increases with increase of the principal quantum number n, scaled as n^2. In addition, the values R_c^I decrease with the increase of Z, scaled as $1/Z$. Also, the R_c^I values decrease with the increase of ionic velocities $v_{\perp 0}$. The influence of parabolic quantum number n_1 (not presented in Table I) can be recognized from the example presented in Fig. 2. In principle, the ionization distances corresponding to a given n decrease with the increase of the first parabolic quantum number n_1. The influence of the quantum number m is similar, but less pronounced.

Accordingly, for the ionization distances $R_c^I(v_{\perp 0})$ presented in Table I, the following estimation can be used:

$$R_c^I = f(v_{\perp 0})R_c, \quad R_c = 2.38\frac{n^2}{Z}, \tag{3.1}$$

where $f(v_{\perp 0})=0.13\exp(-v_{\perp 0}/0.475)+0.88$. The same kind of proportionality between R_c and R_c^I has been obtained in the case of slow hydrogen atoms ($Z=1$, $v_{\perp 0}\approx 0.000\,01$ a.u.) approaching the surface in the presence of a weak external electric field F, discussed within the framework of the EEM in Ref. [20] and, within the framework of the CSM in Ref. [29].

In Fig. 7 we illustrate ionization distances R_c^I (full curves) versus n, Z, and $v_\perp$, Figs. 7(a)–7(c), respectively. In the same figure we also present critical distances R_c (dashed curves). The Fermi distances R_F are presented in Fig. 7(a) by a dot-dashed curve. For comparison with the classical overbarrier model, in Figs. 7(a) and 7(b) we indicate the critical distances R_c^{class} (dotted curves). We recall that $R_c^{class}=2\sqrt{2/Z^3}[1+(Z-1/2)/\sqrt{8Z}]n^2$ [1]. Note that the curves R_c and R_c^{class} are almost equidistant ($\Delta R_c=R_c-R_c^{class}\approx$const), and that the R_c^{class} curves are positioned inside the overbarrier area of Figs. 7(a) and 7(b). To prevent possible confusion, we point out that in the case of electron transfer resonant to Fermi level, a combination of the above expression for R_c^{class} and the condition $E_n=-\phi$ leads to a formula for the critical distance used previously for estimating the neutralization distance of a particular Rydberg level $n=n_c$; see Eq. (22) in Ref. [2] and Eq. (5.11) in Ref. [1].

From Fig. 7 we see that for all considered Rydberg states two different situations appear: $R_c^I > R_c$ and $R_c^I < R_c$, depending on the value of $v_{\perp 0}$. The R_c^I curves for hyperthermal velocity v_1, presented in Figs. 7(a) and 7(b), are above the R_c curves, i.e., they are positioned in the area of subbarrier transitions. On the other hand, other R_c^I curves in these figures are below the R_c curves and correspond to the overbarrier electron transitions. The intersection of the R_c^I (full) curves and R_c (dashed) curves in Fig. 7(c) implies that for certain values n, Z, and $v_{\perp 0}$ ionization distances coincide with the critical distances.

We point out that for $v_{\perp 0}\lesssim 0.01$ a.u. the image acceleration effect is significant. For example, the R_c^I curves for $v_{\perp 0}\equiv v_1=10^{-5}$ a.u., presented in Fig. 7(a), would be lifted by approximately 5 a.u. if the acceleration was neglected. Also, if we were to neglect this effect, instead of $R_c^I\approx R_c$ in the subbarrier area of Fig. 7(c) we would have the increase of R_c^I with the decrease of $v_{\perp 0}$. These conclusions follow from direct numerical calculations based on Eq. (2.19) where the R dependence of the velocity $v_\perp$ is neglected. On the other hand, the same test shows that, in the limiting case of intermediate ionic velocities ($v_{\perp 0}\equiv v_4\approx 1$ a.u.), the image charge acceleration effect is negligible.

The R_c^I curves obtained in the present paper (full curves) for $v_{\perp 0}\approx 1$ a.u. coincide with EEM values from Ref. [18] [symbols ▽ in Figs. 7(a)–7(c)]. Accordingly, in the intermediate-velocity case it is sufficient to use the adaptation of the EEM to the critical region via a two-large-parameter asymptotic [18], which correlates with available beam-foil experimental results. For $v_{\perp 0}\ll 1$ a.u., however, it is necessary to use a more accurate EEM procedure, developed in the present paper.

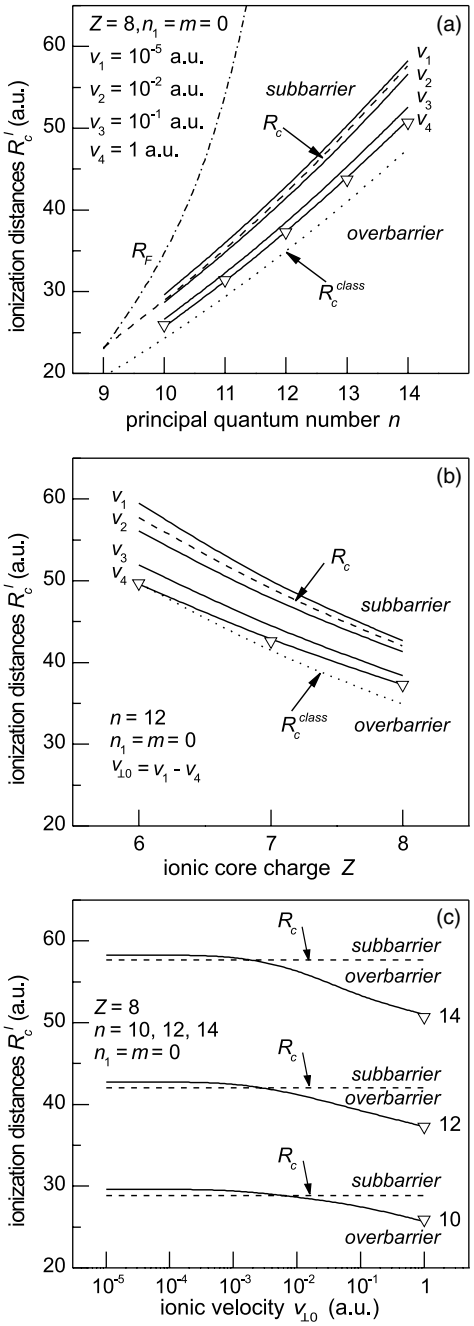

FIG. 7. Ionization distances $R_c^I(n,Z,v_\perp)$ (full curves) expressed via (a) principal quantum number n, (b) ionic core charge Z, and (c) initial ionic velocity $v_{\perp 0}$. Dashed curves correspond to the critical distances $R_c(n,Z)$. Dot-dashed curves correspond the Fermi distances $R_F(n,Z)$ for $\phi=4.2$ eV. The v_1, v_2, v_3, and v_4 values are the same as in Table I. Dotted curves in (a) and (b) are the COB values R_c^{class}[1]. Symbols ▽ in Figs. (a), (b), and (c) represent the ionization distances taken from Ref. [18].

Let us note, finally, that the set of graphs exposed in Fig. 7 has a more general geometrical interpretation; namely, in the space of parameters n, Z, and $v_{\perp 0}$, a surface can be determined which separates the regions of subbarrier and overbarrier electron transitions. All points of that surface, defined by

$$R_c^I(n,Z,v_{\perp 0}) = R_c(n,Z), \tag{3.2}$$

represent a situation where the ionization takes place just "at the top of the effective potential barrier" of the ion-surface system. Accordingly, in the $(n,Z,v_{\perp 0})$ space we can identify a region where electron transitions are mainly of the classically allowed type, as well as a complementary region that is mainly quantum tunneling in character.

IV. CONCLUDING REMARKS

In this paper we calculated the ionization distances R_c^I of one-electron multiply charged Rydberg ions approaching conducting solid surfaces. The R_c^I distances, as well as eigenenergies and rates, are obtained for high-eccentricity states of an active electron, under the condition of image charge acceleration of the ionic projectile $Z \gg 1$, and in the region of low ionic velocities (including the limiting case $v_{\perp 0} \approx 1$ a.u.). The nonperturbative étalon equation method has been applied, which enabled us to identify the contributions of both overbarrier and subbarrier electron transitions near the top of the effective potential barrier of the ion-surface system, around the large critical distance R_c. In the region $R \approx R_c \approx R_c^I$, the parabolic quantum numbers μ can be used as approximate ones, but sufficiently good for a complete classification of decaying states Ψ_μ. This approach represents an extension of the method previously developed for hyperthermal high-eccentricity Rydberg atoms [20]; it is worth noting that the EEM predictions for $Z=1$ are in very good agreement with the results of the complex scaling method [10], as well as with the corresponding experimental data [29,30].

The results for $Z \gg 1$ obtained in the present paper were compared with the available results of the CAM method [7]. This method, however, left unsolved both the R_c^I problem for multiply charged ions and the question of subbarrier and overbarrier contributions. We found that the EEM predictions of the present paper concerning energy terms and rates for $Z=8$ and $n \geqslant 10$ are a complement to the available results of the CAM method; the results of these two methods are in good agreement for $n=n_c=9$ (see Fig. 1). From the EEM presented we can also deduce some conclusions concerning the COB method [1,2,28]; namely, the ionization distances R_c^{class} estimated within the framework of the COB model fall in the overbarrier region [see, for example, Fig. 7(a)], recognized by the EEM. We consider this finding to be nontrivial, because the quantity R_c, determined by Eq. (2.11), and the quantity R_c^{class} have different physical connotations (see Sec. II B).

A few additional concluding comments may be relevant for further investigations of the R_c^I problem of multiply charged ions.

First, the ionization distances R_c^I for parabolic quantum numbers $n_1 \simeq n-1$ and $m \neq 0$ were not discussed in the present paper. These Rydberg states of multiply charged ions, characterized by low eccentricities, are outside our assumption $\xi \ll \eta$, Eq. (2.2), and cannot be consistently treated within the EEM presented. In the large-n_1 case, it can be expected that a wide space region around the projectile trajectory can contribute to the electron exchange process [19]; in addition, electron transitions between adiabatic decaying states must be taken into account. For these reasons, the relevance of various members of the parabolic manifold would require an additional investigation concerning the R_c^I distances of multiply charged ions $Z \gg 1$. We point out that in the $Z=1$ case some experimental data [31] indicate that the R_c^I values of high-lying Xe(n) Stark manifolds are similar for $n_1=0$ and $n_1=n-1$, for $m=0$. A theoretical analysis of this fact, based on the model of avoided crossings, is available [31,32] only for $Z=1$, but not for multiply charged ions $Z \gg 1$.

Second, in the quasistationary model used in the present paper, as well as within the framework of the CSM [10] and CAM method [7], the complete quantum dynamics of the electronic wave function Ψ was not explicitly discussed. Of course, the time evolution of the function Ψ depends on the experimentally imposed initial condition at the time $t=t_{in}$. Accordingly, if the initial electronic state is not determined by parabolic quantum numbers μ (but, for example, by spherical ones ν), the question remains open as to how the state Ψ enters the quasistationary regime of the parabolic type. Under somewhat restrictive conditions, this problem can be treated within the framework of the coupled-channel model, based on the formal expansion of Ψ with respect to an overcomplete solid-ion basis [33].

Third, a "direct observation" of ionization distances R_c^I of multiply charged Rydberg ions approaching solid surfaces would be worthwhile. Up to now, direct observation of R_c^I was experimentally performed only for neutral Rydberg atoms $(Z=1)$ [29,30] and H_2 molecules [34] slowly approaching solid surfaces. These experimental methods are based on the fact that a neutral projectile, after undergoing the ionization process, can be decelerated and stopped along the path toward the surface by a weak external electric field, and sent back into a detector. In contrast to such an observation of R_c^I for initially neutral systems, the situation with $Z \gg 1$ is somewhat different because the projectiles are charged from the very beginning and because of relatively strong image accelerations toward the surface.

Finally, bearing in mind the above mentioned (both theoretical and experimental) perplexities, it is a challenging task to consider the R_c^I problem by taking into account that the R_c^I values depend on both initial and final states of an active electron. This can be done within the framework of two-state vector formalism, without using the overcomplete basis expansion; for the structure of this method, in the context of the ion-surface interaction, see Refs. [16–19]. In this approach, the active electron is simultaneously described by two wave functions $\Psi_\nu^{(1)}$ and $\Psi_\mu^{(2)}$ at any instant of time t. Consequently, we have $R_c^I = R_c^I(\mu,\nu)$ so that a somewhat different insight into the R_c^I problem is possible.

ACKNOWLEDGMENT

This work was supported in part by the Ministry of Science and Environmental Protection, Republic of Serbia (Project No. 14 1029).

[1] J. Burgdörfer, in *Review of Fundamental Processes and Applications of Atoms and Molecules*, edited by C. D. Lin (World Scientific, Singapore, 1993).
[2] J. Burgdörfer, P. Lerner, and F. W. Meyer, Phys. Rev. A **44**, 5674 (1991).
[3] J. J. Ducrée, F. Casali, and U. Thumm, Phys. Rev. A **57**, 338 (1998).
[4] J. Ducrée, H. J. Andrä, and U. Thumm, Phys. Rev. A **60**, 3029 (1999).
[5] U. Wille, Phys. Rev. B **50**, 1888 (1994).
[6] D. Teillet-Billy and J. Gauyacq, Surf. Sci. **239**, 343 (1990).
[7] A. G. Borisov, R. Zimny, D. Teillet-Billy, and J. Gauyacq, Phys. Rev. A **53**, 2457 (1996).
[8] P. Nordlander and J. C. Tully, Phys. Rev. Lett. **61**, 990 (1988).
[9] P. Nordlander and J. C. Tully, Phys. Rev. B **42**, 5564 (1990).
[10] P. Nordlander, Phys. Rev. B **53**, 4125 (1996).
[11] J. Hanssen, C. F. Martin, and P. Nordlander, Surf. Sci. **423**, L271 (1999).
[12] V. A. Mandelshtam, T. R. Ravueri, and H. S. Taylor, Phys. Rev. Lett. **70**, 1932 (1993).
[13] J. Muller, X. Yang, and J. Burgdörfer, Phys. Rev. A **49**, 2470 (1994).
[14] P. Kürpick and U. Thumm, Phys. Rev. A **54**, 1487 (1996).
[15] P. Kürpick, U. Thumm, and U. Wille, Phys. Rev. A **57**, 1920 (1998).
[16] N. N. Nedeljković, Lj. D. Nedeljković, S. B. Vojvodić, and M. A. Mirković, Phys. Rev. B **49**, 5621 (1994).
[17] Lj. D. Nedeljković and N. N. Nedeljković, Phys. Rev. B **58**, 16455 (1998).
[18] Lj. D. Nedeljković and N. N. Nedeljković, Phys. Rev. A **67**, 032709 (2003).
[19] N. N. Nedeljković, Lj. D. Nedeljković, and M. A. Mirković, Phys. Rev. A **68**, 012721 (2003).
[20] N. N. Nedeljković and Lj. D. Nedeljković, Phys. Rev. A **72**, 032901 (2005).
[21] S. Y. Slavyanov, in *Problems in Mathematical Physics*, edited by M. S. Birman (Leningrad State University Press, Leningrad, 1970), Vol. 4, p. 125 (in Russian).
[22] S. Y. Slavyanov, Diff. Eq. **5**, 313 (1969) (in Russian).
[23] V. Kolosov, J. Phys. B **16**, 25 (1983).
[24] D. C. Langerth and P. Nordlander, Phys. Rev. B **41**, 2541 (1991).
[25] N. N. Nedeljković, R. K. Janev, and V. Yu. Lazur, Phys. Rev. B **38**, 3088 (1988).
[26] P. Appel, Nucl. Instrum. Methods Phys. Res. B **23**, 242 (1987).
[27] N. N. Nedeljković, Fizika (Zagreb) **12**, 275 (1980).
[28] J. Burgdörfer and F. Meyer, Phys. Rev. A **47**, R20 (1993).
[29] S. B. Hill, C. B. Haich, Z. Zhou, P. Nordlander, and F. B. Dunning, Phys. Rev. Lett. **85**, 5444 (2000).
[30] S. Wethekam, H. R. Dunham, J. C. Lancaster, and F. B. Dunning, Phys. Rev. A **73**, 032903 (2006).
[31] Z. Zhou, C. Oubre, S. B. Hill, P. Nordlander, and F. B. Dunning, Nucl. Instrum. Methods Phys. Res. B **193**, 403 (2002).
[32] F. B. Dunning, H. Dunham, C. Oubre, and P. Nordlander, Nucl. Instrum. Methods Phys. Res. B **203**, 69 (2003).
[33] J. Burgdörfer, E. Kupfer, and H. Gabriel, Phys. Rev. A **35**, 4963 (1987).
[34] G. R. Lloyd, S. P. Procter, and T. P. Softley, Phys. Rev. Lett. **95**, 133202 (2005).